Molecular Biology of the Cell
Vol. 20, 400–409, January 1, 2009

Cytoskeletal Tropomyosin Tm5NM1 Is Required for Normal Excitation–Contraction Coupling in Skeletal Muscle

Nicole Vlahovich,*†‡§ Anthony J. Kee,*‡‖ Chris Van der Poel,¶ Emma Kettle,* Delia Hernandez-Deviez,# Christine Lucas,*@ Gordon S. Lynch,¶ Robert G. Parton,# Peter W. Gunning,‖@ and Edna C. Hardeman*††**

*Muscle Development Unit, Children's Medical Research Institute, Westmead, NSW, Australia; †University of Western Sydney, Parramatta, NSW, Australia; ‖Faculty of Medicine, University of Sydney, Sydney, NSW, Australia; ¶Department of Physiology, University of Melbourne, Parkville, VIC, Australia; #Institute for Molecular Biosciences, University of Queensland and Centre for Microscopy and Microanalysis, Brisbane, QLD, Australia; @Oncology Research Unit, The Children's Hospital at Westmead, Westmead, NSW, Australia; **Department of Pharmacology, School of Medical Sciences, University of New South Wales, Sydney, NSW, Australia; and ††Department of Anatomy, School of Medical Sciences, University of New South Wales, Sydney, NSW, Australia

Submitted June 18, 2008; Revised October 17, 2008; Accepted October 31, 2008
Monitoring Editor: Thomas D. Pollard

The functional diversity of the actin microfilaments relies in part on the actin binding protein tropomyosin (Tm). The muscle-specific Tms regulate actin-myosin interactions and hence contraction. However, there is less known about the roles of the numerous cytoskeletal isoforms. We have shown previously that a cytoskeletal Tm, Tm5NM1, defines a Z-line adjacent cytoskeleton in skeletal muscle. Recently, we identified a second cytoskeletal Tm in this region, Tm4. Here we show that Tm4 and Tm5NM1 define separate actin filaments; the former associated with the terminal sarcoplasmic reticulum (SR) and other tubulovesicular structures. In skeletal muscles of Tm5NM1 knockout (KO) mice, Tm4 localization was unchanged, demonstrating the specificity of the membrane association. Tm5NM1 KO muscles exhibit potentiation of T-system depolarization and decreased force rundown with repeated T-tubule depolarizations consistent with altered T-tubule function. These results indicate that a Tm5NM1-defined actin cytoskeleton is required for the normal excitation–contraction coupling in skeletal muscle.

INTRODUCTION

The tropomyosin (Tm) family of actin-binding proteins consists of >40 isoforms generated by alternate RNA splicing from four mammalian genes. Tm dimers bind the α-helical groove of the actin filament in a head-to-tail orientation and are important components of the actin microfilament cytoskeleton (Perry, 2001). The Tm isoforms function in a variety of different cellular pathways in a range of cell and tissue types and are developmentally regulated (Gunning *et al.*, 2008). In skeletal muscle, Tm isoforms function as a component of the contractile apparatus, regulating the actin–myosin interaction to facilitate sarcomeric contraction. Only three striated muscle Tm isoforms are required to fulfil this function; whereas the majority of the Tm isoforms are used by the actin cytoskeleton and contribute to the diversity of actin filament function (Gunning *et al.*, 2008).

Tm isoforms are functionally distinct and sort to specific compartments within the cell (Gunning *et al.*, 2008). Studies show that Tm isoforms protect actin filaments in an isoform-specific manner from the severing action of gelsolin (Ishikawa *et al.*, 1989) and depolymerization by ADF/cofilin (Bernstein and Bamburg, 1982; Ono and Ono, 2002; Bryce *et al.*, 2003). Tm isoforms can differentially regulate myosin enzymology and mechanochemistry (Fanning *et al.*, 1994) and also the sorting of myosin motors (Tang and Ostap, 2001; Bryce *et al.*, 2003). This compartmentalization is best described in neuronal cells (reviewed in Gunning *et al.*, 2008). During neuronal development, specific Tm isoforms sort to the axonal shaft and growth cone. On differentiation, additional Tm isoforms are expressed and Tms relocalize to form distinct compartments in the axon, soma, dendrite, and presynaptic terminals (Had *et al.*, 1993; Weinberger *et al.*, 1993; Hannan *et al.*, 1995, 1998; Schevzov *et al.*, 1997). This compartmentalization is not restricted to neuronal cells. During the G1 phase of the cell cycle in fibroblasts, some Tm isoforms locate to stress

This article was published online ahead of print in *MBC in Press* (http://www.molbiolcell.org/cgi/doi/10.1091/mbc.E08–06–0616) on November 12, 2008.

‡ These authors contributed equally to this work.

§ Present address: The Burnham Institute for Medical Research, 10901 North Torrey Pines Rd., La Jolla, CA 92037.

Address correspondence to: Edna C. Hardeman (e.hardeman@unsw.edu.au).

Abbreviations used: DHPR, dihydropyridine receptor; DICR, depolarization-induced contractile response; EDL, extensor digitorum longus; EM, electron microscopy; FDB, flexor digitorum brevis; KO, knockout; MyHC, myosin heavy chain; SR, sarcoplasmic reticulum; Tm, tropomyosin; WT, wild type.

Supplemental Material can be found at:
http://www.molbiolcell.org/content/suppl/2008/11/12/E08-06-0616.DC1.html

fibers, whereas Tm5NM2 remains associated with the Golgi (Percival *et al*., 2004) and additional isoforms containing the γ-*TM* gene 9a exon localize to a perinuclear compartment (Schevzov *et al*., 2005a). Similar phenomena have been described in epithelial cells, in which Tm5a and 5b localize to the apical surface of cultured cells, Tm2 and Tm3 are present at the basolateral membrane and isoforms generated from the γ-*TM* gene are found in the central cytoplasm (Dalby-Payne *et al*., 2003). Sorting of functionally distinct Tm isoforms provides a mechanism for the spatial regulation of different actin filament populations.

Cytoskeletal Tm isoforms also have been detected in striated muscle. We demonstrated previously that a cytoskeletal Tm from the γ-*TM* gene, Tm5NM1, localizes to the sarcolemma and to a region adjacent to the Z-line in skeletal muscle fibers (Kee *et al*., 2004). In addition, we have shown that Tm4, the single product of the δ-*TM* gene, is also found in this region and in longitudinal filaments in regenerating or repairing muscle (Vlahovich *et al*., 2008). Both Tm5NM1 and Tm4 colocalize with a γ-actin cytoskeleton at these sites, suggesting a role for these filament systems in stabilization of the muscle fibers and linking myofibrillar networks to the membrane systems. In this study, we show that Tm5NM1 and Tm4 define separate filament systems and that Tm4 associates with the terminal sarcoplasmic reticulum and other tubulovesicular structures in the I-band and other regions of the muscle. Ablation of Tm5NM1 expression in the skeletal muscles of a γ-*TM* exon 9d knockout (KO) mouse indicates that Tm5NM1 plays a role in maintenance of normal excitation–contraction coupling.

MATERIALS AND METHODS

Antibodies

Tm isoform-specific antibodies are described in Schevzov *et al*. (2005b): γ9d (sheep polyclonal antibody) recognizes the 9d exon from the γ-*TM* gene corresponding to Tm5NM1 in skeletal muscle and WD4/9d (rabbit polyclonal antibody) recognizes Tm4. Other primary antibodies used were: dihydropyridine receptor (mouse monoclonal, MAB47; Millipore Bioscience Research Reagents, Temecula, CA) and calsequestrin (mouse monoclonal, clone 51; BD Biosciences, Franklin Lakes, NJ). Secondary antibodies used were 488-conjugated goat anti-rabbit, 594-conjugated goat anti-mouse, and 594-conjugated donkey anti-sheep (Alexa Fluor; Invitrogen, Carlsbad, CA). Goat anti-rabbit and goat anti-mouse horseradish peroxidase (HRP)-conjugated antibodies (Bio-Rad, Hercules, CA) were used for Western blot analysis.

Mice

All animal experiments were performed in accordance with institutional and National Health and Medical Research Council guidelines. Mice were generated as described in Schevzov *et al*. (2008). A knockout construct was designed to specifically delete exon 9d-containing isoforms from the γ-*TM* gene. Targeted 129X1/SvJ ES cells were used to generate heterozygous mice (129X1/SvJ background; Tm5/9dneo mice). The same KO construct was electroporated into Bruce 4 C57Bl/6 ES cells. Heterozygous mice (C57Bl/6 background) were bred with mice carrying a cytomegalovirus-Cre recombinase transgene (C57Bl/6 background) (Schwenk *et al*., 1995) and then bred onto the C57Bl/6JArc background (Tm5/9d/89 mice) for >10 generations. All data presented is from mice of the Tm5/9dneo line and corresponding wild-type strain (129X1SvJ) unless otherwise indicated. All studies were performed on 2- to 3-mo-old male mice, and control wild-type (WT) mice were aged matched to within 1 wk of the KO mice.

Immunohistochemistry

Mouse muscles were fixed in 4% paraformaldehyde (PFA) (hindlimb muscles were stretched and held during fixation) and infused with 1.8 M sucrose/20% polyvinylpyrrolidone as described by Vlahovich *et al*. (2008). Semithin (0.5- to 0.8-μm) sections were cut at −60°C using an Ultracut UCT ultramicrotome (Leica, Wetzler, Germany) equipped with an EM FCS cryochamber (Leica). Sections were blocked and incubated with primary (γ9d, 1:50; α-actinin, 1:500) and secondary antibodies (goat anti-mouse, 1:2000; donkey anti-sheep 1:1000) and viewed using either a confocal laser scanning microscope (oil immersion 63× objective, model TCS SP2; Leica) or standard fluorescent microscopy (BX51 microscope; Olympus, Tokyo, Japan).

Immunogold Labeling

Extensor digitorum longus (EDL) muscles were fixed in 4% PFA/0.1% glutaraldehyde/phosphate buffer, pH 7.2, for 1 h. Ultrathin cryosections were prepared according to Griffiths *et al*. (1984).

Immunogold labeling was carried out on an EM IGL Automated Immunogold Labeling System (Leica). Grids were blocked for 15 min in 50 mM glycine, 30 min in protein block, and incubated in primary antibodies (Tm4, 1:75; calsequestrin, 1:2000) diluted in immunoincubation buffer (0.25% bovine serum albumin [BSA]/12.5 mM sodium azide/phosphate-buffered saline [PBS], pH 7.4) overnight at 4°C. Grids were washed in immunoincubation buffer, incubated in gold-conjugated secondary antibodies (protein A gold 5 nm or goat anti-rabbit 10 nm gold [1:20], goat anti-mouse 20 nm gold [1:20] diluted in immunoincubation buffer; British BioCell International, Cardiff, United Kingdom) for 2 h at room temperature, washed in immunoincubation buffer, and fixed in 2% glutaraldehyde/PBS for 5 min. Grids were washed in PBS and water, and then they were embedded for 15 min in 1% methylcellulose:3% aqueous uranyl acetate diluted 9:1. Immunolabeled tissue was examined on a Philips CM10 transmission electron microscope. Quantitation of Tm4 and calsequestrin immunogold label was performed on three different grids with 10 random fields (each field containing at least 1 typical triad structure) counted per grid. The number of gold particles on each structure was counted as a percentage of the total number of gold particles in the whole field, and an average of the 10 fields/grid was calculated. Data are represented as mean ± SEM of the counts from the three grids/mouse line.

Isolation of Membrane Fractions

Membrane fractions from skeletal muscle were isolated using the method described by Saito *et al*. (1984). Membrane fractions at the interfaces between the discontinuous sucrose gradients (45, 38, 32, 27% sucrose) were collected, centrifuged for 2 h at 20,000 × g_{max} and the pellets were processed for cryo-electron microscopy (EM) for immunogold labeling.

Muscle Fiber Isolation and Analysis for Immunohistochemistry

Isolated muscle fibers from flexor digitorum brevis (FDB) muscle were isolated and cultured as described previously (Hernandez-Deviez *et al*., 2006). Primary (γ9d, 1:50; Tm4, 1:200; dihydropyridine receptor [DHPR], 1:200) and secondary (goat anti-mouse, 1:2000; goat anti-rabbit, 1:1000; donkey anti-sheep, 1:1000) antibody incubations were carried out at 37°C for 60 min or overnight at 4°C. Fibers were mounted and viewed using an LSM 510 META confocal microscope system (Carl Zeiss, Sydney, NSW, Australia). Single optical sections were captured using a Plan apochromatic 63× 1.4 numerical aperture oil immersion objective.

Detection and Quantitation of T-Tubule Dysmorphology

EDL muscles were fixed overnight in Karnovsky's fixative, processed in a LYNX tissue processor (Electron Microscopy Sciences, Hatfield, PA), and embedded in TAAB low viscosity resin. Ultrathin sections were stained with uranyl acetate and lead citrate and viewed in a Phillips CM10 transmission electron microscope. The T-tubule dysmorphology was calculated from a total of 1000 junctional membrane structures from muscles of at least three different mice of each genotype (Komazaki *et al*., 2003).

Western Blot Analysis

Protein extracts from mouse muscle were prepared and 12.5% SDS-polyacrylamide gel electrophoresis (PAGE) gels run as described by Kee *at al*. (2004). Coomassie-stained gels were used to verify equal protein loading. Protein was transferred onto polyvinylidene difluoride membranes (Millipore, Sydney, NSW, Australia), blocked in skim milk and incubated with primary (CG3, 1:1000; Tm4, 1:500; γ9d, 1:500) and secondary antibodies (HRP-labeled secondary 1:10,000) according to Kee *et al*. (2004). Protein detection was performed using the SuperSignal West Pico chemiluminescence kit (Pierce Chemical, Rockford, IL).

Myosin Heavy Chain (MyHC) Isoform Gel Electrophoresis

MyHC isoform composition of EDL muscle was determined as described by Nair-Shalliker *et al*. (2004).

In Vivo Strength Tests

Whole animal strength and fatigability were measured according to the test procedure outlined in Joya *et al*. (2004). In brief, this test required the mice to pull themselves on top of a suspended rod with muscle weakness based on the mean percentage of passes over 15 trials in 3 min. Forearm strength was assessed using a dynamometer constructed according to the design of Smith *et al*. (1995). The mouse is suspended by the tail and the mouse grasps a horizontal bar. The bar is steadily moved away from the animal with increasing force and the force with which the animal releases the bar and the time taken for this to occur is recorded. This is repeated 10 times/mouse for four consecutive days and the last 2 day's readings are averaged.

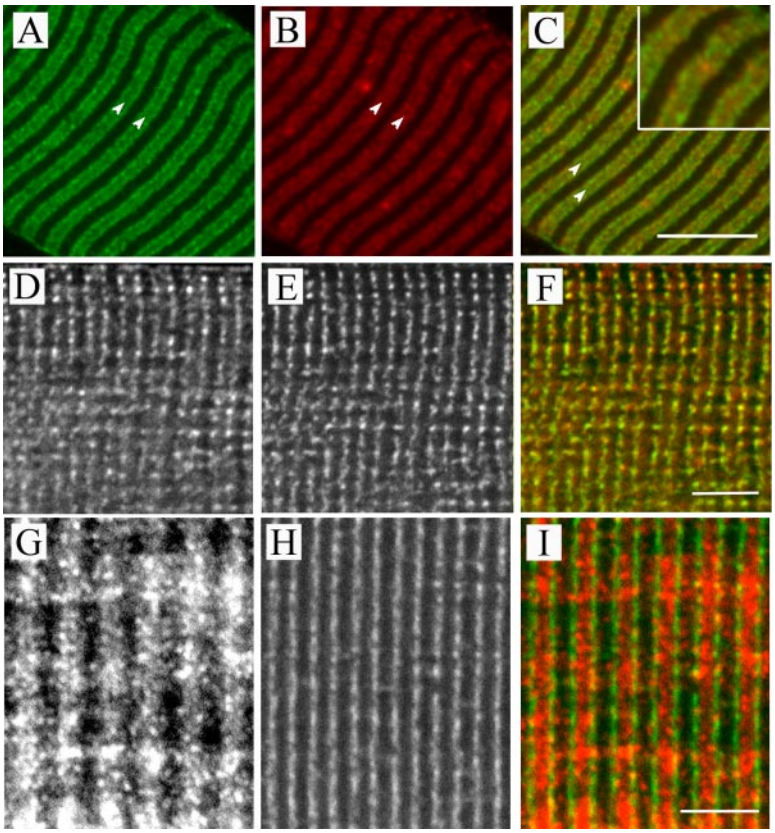

Figure 1. Tm5NM1 and Tm4 are located in distinct regions in skeletal muscle. (A–C) Semithin sections (0.5 μm) of stretched soleus muscle costained with Tm5NM1 (A) and Tm4 (B) antibodies; merged image in C. Although Tm5NM1 and Tm4 are located in a similar Z-line adjacent region (Z-lines indicated by arrowheads) the signals do not colocalize (see higher magnification of C in the insert). (D–I) Tm5NM1 (D and F, red) and Tm4 (G and I, red) localization was determined in isolated FDB muscles fibers with respect to the T-tubule constituent, the DHPR (E and H). Confocal microscopy shows that Tm5NM1 colocalizes with the T-tubule marker DHPR shown by the presence of yellow in the merge image (F), whereas Tm4 did not (I). Bars (C, F, and I), 5 μm.

Isolated Muscle Contractile Measurements

EDL muscles were carefully removed tendon-to-tendon from anesthetized (100 mg/kg body weight ketamine/10 mg/kg body weight xylazine), 10- to 12-wk-old mice for in vitro contractile measurements according to the method of Gregorevic *et al*. (2004). Optimal muscle length was determined with digital calipers during a series of isometric twitch contractions. Maximum isometric tetanic force was determined from the plateau of the frequency-force curve (1–200 Hz) and expressed as force/cross-sectional area (CSA). CSA was determined as described previously (Lynch *et al*., 2001).

Single Fiber Contractile Measurements

Single mechanically skinned fibers were prepared as described by Stephenson and Williams (1981). Mechanically skinned fibers were attached at one end to a piezoresistive force transducer (AE801; SensoNor, Horten, Norway), and the other end was fixed to a micromanipulator. Determination of the sarcoplasmic reticulum (SR) properties has been described previously (van der Poel and Stephenson, 2007). Ca^{2+} release from the SR was estimated from the relative areas under the caffeine-induced force response (CIFR) (van der Poel and Stephenson, 2007). Because the area under the CIFR is proportional to the SR loading times, the relative area under the CIFR was used to estimate the amount of Ca^{2+} in the SR (van der Poel and Stephenson, 2007). The percentage of Ca^{2+} lost from the SR due to the passive leak over a 60-s period was also assessed (van der Poel and Stephenson, 2007). After measurement of SR function the properties of the contractile apparatus were examined. Fibers were placed in a maximum Ca^{2+}-activating solution (pCa $\sim$ 4.5) to obtain maximum Ca^{2+}-activated force. Fibers were then exposed to activating solutions of progressively higher [Ca^{2+}], and the force response generated at each pCa was expressed as a percentage of the interpolated values for maximum Ca^{2+}-activated force (van der Poel and Stephenson, 2002). Data points were fitted with a Hill equation producing two parameters: the pCa_{50} (i.e., pCa that produces half-maximum force) and the n_H (i.e., the Hill coefficient, indicative of the steepness of the force–pCa relationship).

Depolarization-induced contractile responses (DICR) were also performed to examine T-tubule function (Plant and Lynch, 2002). Mechanically skinned muscle fibers were polarized with potassium hexamethylenediamine-tetraacetic acid (HDTA). The T-tubular membrane system was then depolarized with Na-HDTA, causing a transient DICR. Muscle fibers were then repolarized with K-HDTA before eliciting another Na-HDTA depolarization. This protocol was repeated to produce DICRs until the peak amplitude of the DICR had reached <50% of the initial value.

Statistical Analysis

Statistical significance was tested at $p < 0.05$ levels using Student's *t* test.

RESULTS

The Z-Line Adjacent Actin Cytoskeleton Is Composed of at Least Two Distinct Cytoskeletal Systems Defined by Different Tm Isoforms

We previously identified actin filament systems defined by cytoskeletal Tms, Tm4 and Tm5NM1 in skeletal muscle cells (Kee *et al*., 2004; Vlahovich *et al*., 2008). To determine whether Tm5NM1 and Tm4 are present in the same filament or define distinct filamentous populations and whether they are associated with organelles in the Z-line region, colocalization studies were performed. Costaining of stretched soleus muscle with the Tm-specific antibodies shows that Tm4 and Tm5NM1 occupy similar Z-line adjacent positions (Figure 1, A–C). However, the staining of the two Tms is not identical; Tm4 has some staining over the Z-line, whereas Tm5NM1 seems to localize exclusively to the Z-line adjacent region.

In skeletal muscle, two membrane systems that regulate calcium entry, the T-tubules and the SR, meet adjacent to the Z-line to form triads. An antibody to a well-characterized marker of the T-tubule system the DHPR was used to investigate a potential relationship between the triads and Tm4 or Tm5NM1. Single muscle fibers from the FDB muscle were isolated and incubated with antibodies to DHPR and either Tm5NM1 or Tm4. Single fiber preparations were chosen as they provide higher resolution of myofiber structures than muscle cryosections. Using this approach, Tm5NM1 shows a striking colocalization with the DHPR (Figure 1, D–F). In

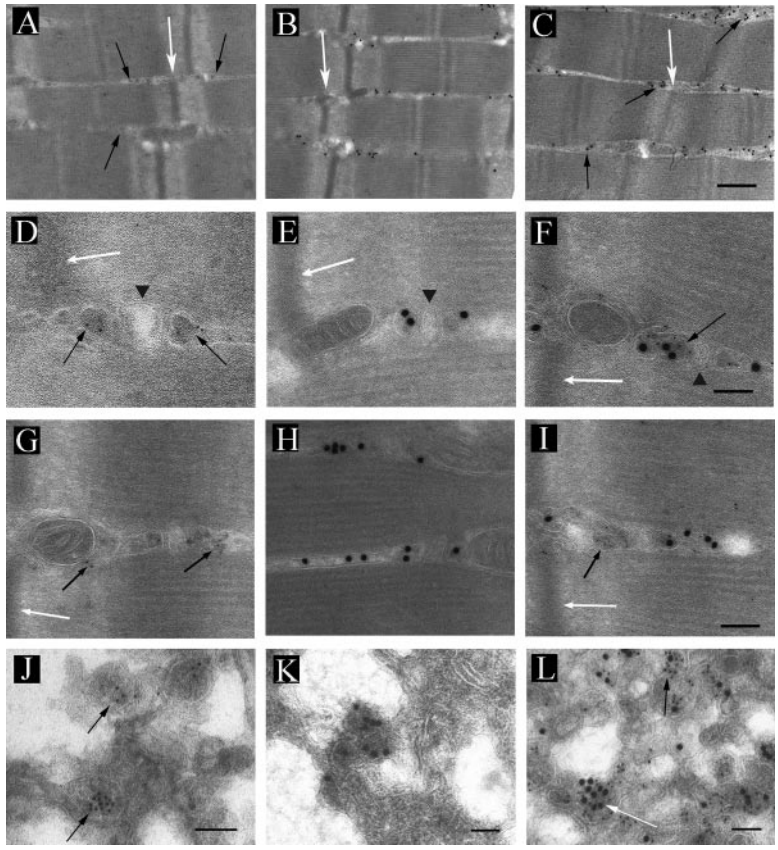

Figure 2. Tm4 localizes to the terminal SR and other tubulovesicular structures. (A–I) Immunogold labeling of Tm4 (5-nm gold; A, D, and G) and calsequestrin (20-nm gold; B, E, and H) in EDL muscle from WT mice. D–F are regions of A–C at higher magnification. Immunogold detection using Tm4 antibodies shows that Tm4 localizes to terminal SR membranes of the triad (A and D, black arrows) but not the T-tubule membranes (arrowheads, D–F). Colabeling of sections with calsequestrin (C and F) shows that both Tm4 (5-nm gold, black arrows) and calsequestrin (20-nm gold) localize to the same region at the SR membrane. Tm4 was also localized to other nontriad membranes in the I- and A-bands (G and I, black arrows). White arrows in A–G and I mark the Z-lines. A–C are the same magnification. Bar (C), 500 nm. D–I are the same magnification. Bar (F and I), 100 nm. (J–L) SR membrane fractions were also generated by ultracentrifugation to further examine the localization of Tm4 by immuno-EM. Immunogold labeling of Tm4 by using 10-nm gold (J, arrows) and calsequestrin with 20-nm gold (K) revealed labeling of terminal SR vesicles. Double labeling using both antibodies (L) showed that Tm4 (black arrow) and calsequestrin (white arrow) label the same vesicles. Bars (J–L), 100 nm.

contrast, Tm4 has a broader staining pattern independent of the DHPR (Figure 1, G–I). The more restricted staining pattern of Tm5NM1 compared with Tm4 in the single fibers is in agreement with the semithin sections (Figure 1, A–C) indicates that they have overlapping but not identical distributions in muscle.

To gain further insight into Tm4 localization, immunogold labeling and EM was performed on frozen sections of mouse EDL muscle (Figure 2). Immunolabeling of EDL sections showed that Tm4 localizes mainly to the sarcoplasmic reticulum and tubulovesicular structures around the triad region of the I-band (Figure 2, A, D, and G; black arrows). To confirm the identity of the SR localization, muscle sections were labeled for calsequestrin, a marker of the terminal cisternae of the SR (Figure 2, B, E, and H). Colabeling of the sections showed that Tm4 and calsequestrin colocalize to the same membrane systems (Figure 2, C, F, and I). To determine the exact localization of Tm4, quantitation of gold particles was performed on WT muscle (Table 1). The quantitative data demonstrates that calsequestrin and Tm4 local-

Table 1. Quantitation of Tm4-associated structures in skeletal muscle by immunoelectron microscopy

	Wild type		Knockout	
	Calsequestrin	Tm-4	Calsequestrin	Tm-4
Terminal SR[a]	27.25 ± 0.27	22.40 ± 3.27	28.95 ± 0.60	20.09 ± 1.73
SR/tubulovesicular[b]	71.61 ± 0.23	42.10 ± 6.50	66.92 ± 1.66	42.38 ± 6.07
I-band[c]	0.40 ± 0.05	8.76 ± 1.37	1.39 ± 0.84	11.29 ± 2.82
A-band[d]	0.26 ± 0.26	24.69 ± 5.12	2.47 ± 1.45	24.30 ± 4.53
T-tubules	0.48 ± 0.28	0.00 ± 0.00	0.21 ± 0.21	0.00 ± 0.00
Z-line	0.00 ± 0.00	2.05 ± 0.31	0.05 ± 0.05	1.94 ± 0.59

The number of gold particles in each region as a percentage of the total number of gold particles is shown. Values are mean ± SEM of three electron microscope grids with 10 regions/grid counted. There is no statistical difference (ANOVA) between WT and KO muscle for the percentage of gold label associated with any of the muscle structures for Tm4 or calsequestrin.

[a] Terminal cisternae of the sarcoplasmic reticulum in apposition to the t-tubules.

[b] Tubulovesicular structures or sarcoplasmic reticulum in the I-band region excluding the terminal SR.

[c] I-band nonmembrane bound.

[d] A-band nonmembrane bound.

ize to the same structures with approximately 30% of calsequestrin and 22% of Tm4 found on the terminal SR membranes, and approximately 70% of calsequestrin and 42% of Tm4 on tubulovesicular structures or sarcoplasmic reticulum in the I-band region (Table 1). No Tm4 labeling was detected on the T-tubules. These results indicate that the Tm4-defined cytoskeleton is in close association with the SR membrane system. Some Tm4 label was also found on nonmembranous areas of the A- and I-bands (Table 1). Some of this label could be nonspecific but some of the A-band label may be associated with longitudinal Tm4 filaments that we have described previously (Vlahovich *et al*., 2008). A primary antibody omission negative control for each antibody demonstrated no label for the calsequestrin control and a mean of 0.7 gold particles per field for the Tm4 control (data not shown).

To assign a more precise localization of Tm5NM1 immunogold labeling of WT muscle was also attempted using the Tm5NM1-specific antibody γ9d. Unfortunately, no specific labeling was observed perhaps due to the low abundance of Tm5NM1 in muscle (Kee *et al*., 2004). To overcome this problem, immuno-EM was performed on muscle from a Tm5NM1 transgenic mouse line (Tm5/52) that expresses the human protein at >5 times the endogenous protein (Schevzov *et al*., 2005a). Unfortunately, again no specific labeling was observed.

Tm4 association to SR membranes was also examined by muscle cell membrane fractionation. Membrane fractions were generated by ultracentrifugation of homogenates of pooled hindlimb muscle through a discontinuous sucrose gradient. The pellet of the SR fraction (fraction 4) was processed for immuno-EM. This fraction has been shown previously to be enriched for the terminal SR membranes (Saito *et al*., 1984). Immuno-EM staining of Tm4 and calsequestrin revealed the presence of Tm4 associated with calsequestrin containing vesicles (Figure 2, J–L) confirming that Tm4 is associated with the terminal SR.

Other Tm Isoforms from the γ-TM Gene and Tm4 Do Not Compensate for the Absence of Tm5NM1 in KO Mice

To examine the role of Tm5NM1 in skeletal muscle fibers, we analyzed mice that are null for Tm5NM1 and Tm5NM2 (Schevzov *et al*., 2008). Because Tm5NM2 is not expressed in skeletal muscle (Kee *et al*., 2004; Percival *et al*., 2004), these mice allow us to study the role of Tm5NM1, exclusively, in skeletal muscle. Using the γ9d antibody that recognizes Tm5NM1 and Tm5NM2, Western blotting was performed on EDL and FDB muscles to confirm the absence of Tm5NM1 protein in KO muscles (Figure 3A). Using an antibody (CG3) that recognizes the 1b exon of the γ-*TM* gene, present in all cytoskeletal isoforms from this gene, we found that other γ-*TM* gene isoforms are not up-regulated to compensate for the lack of Tm5NM1 in skeletal muscle (Figure 3A). The typical localization of Tm5NM1 at the Z-line adjacent region of EDL muscle (Figure 3B) is lost in skeletal muscle from KO mice (Figure 3C). However, the localization of Tm4 to the terminal SR (black arrows in Figure 3D) and other membrane and nonmembranous structures remained unchanged in the absence of Tm5NM1 (Figure 3 and Table 1).

Tm5NM1 KO Mouse Muscles Display T-Tubule Dysmorphology

EDL muscles from Tm5NM1 KO mice were analyzed by EM to determine whether the absence of Tm5NM1 impacts on the morphology of the T-tubules (Komazaki *et al*., 2003). Triads were examined for alterations to T-tubule structure (Figure 4). The level of T-tubule dysmorphology was increased in Tm5NM1 KO muscle (Figure 4, B and C) in comparison with WT muscles (Figure 4A). In electron micrographs, the T-tubule shows up as a membrane structure orientated in parallel to the Z-line (Figure 4A, T-tubules labeled by an asterisk, SR by black arrows, and Z-line by white arrow) and flanked by the terminal SR. The T-tubules were considered abnormal if they were orientated diagonally (Figure 4B, asterisk) or were bent or crooked (Figure 4C, asterisk). Quantitation of T-tubule dysmorphology was performed on a total of 1000 junctional structures from WT and KO muscle per mouse (Figure 4D). We found a small but significant increase (3.2 times) in morphologically abnormal T-tubules in the KO muscle compared with WT skeletal muscle.

Tm5NM1 KO Mouse Muscles Have Altered Muscle Contractile Properties

To determine the functional consequences of Tm5NM1 ablation, we determined the contractile properties of isolated intact EDL muscles from homozygous KO mice (Tm5/9dneo line) and WT mice of the same background strain (129X1/SvJ) (Figure 5). The same measurements were made on the second Tm5NM1 KO line (Tm5/9d/89) and its WT control mice (C57Bl/6JArc strain) with essentially the same results (Supplemental Figure 1). There was a significant increase in specific twitch force (single stimulus) (Figure 5A), but not maximum tetanic force (stimulation frequency, 150 Hz) (Figure 5B) in the EDL muscles from the KO mice compared with WT controls. This was also evident in the stimulation frequency–force relationship where force was greater in the KO muscle at low stimulation frequencies ($\leq$30 Hz, $p < 0.05$), but not higher frequencies (Figure 5E). At physiological stimulation frequencies (75–100 Hz for the EDL) force output from the KO muscle was not different from WT muscle. This is consistent with the lack of improved muscle strength in this mouse (whole body muscle strength and fatigability test and forearm grip strength; Supplemental Figure 2). The time to reach peak twitch contraction was also more rapid in the KO muscle (Figure 5C), but relaxation time was similar to WT muscle (Figure 5D). Lack of an effect on contraction relaxation time is an indication that Ca^{2+} reuptake from the SR is not altered in the KO mice. Taken together, the data are consistent with either an increase in Ca^{2+} release from the SR with each single activation or alteration to T-tubule function in the KO mice such that each electrical stimulus leads to greater T-tubule activation and increased twitch force.

Altered Contractile Properties in Tm5NM1 KO Muscle Is Not Due to Fiber-Type Changes

Slower fibers reach maximum force output at lower stimulation frequencies. To examine whether a fast-to-slow fiber-type shift was responsible for the leftward shift in the frequency force curve in the KO muscle we analyzed the MyHC isoform composition of EDL muscles from KO and WT mice by SDS-PAGE (Figure 6). EDL muscles from mice typically express predominantly the fast MyHC isoforms 2B, 2X, and 2A. There was no difference in the amount of each isoform in KO and WT muscles (Figure 6B). From this analysis it is apparent that MyHC composition is unchanged in the KO muscle indicating that the altered contractile properties of the KO muscle was not a consequence of changes in muscle fiber type composition.

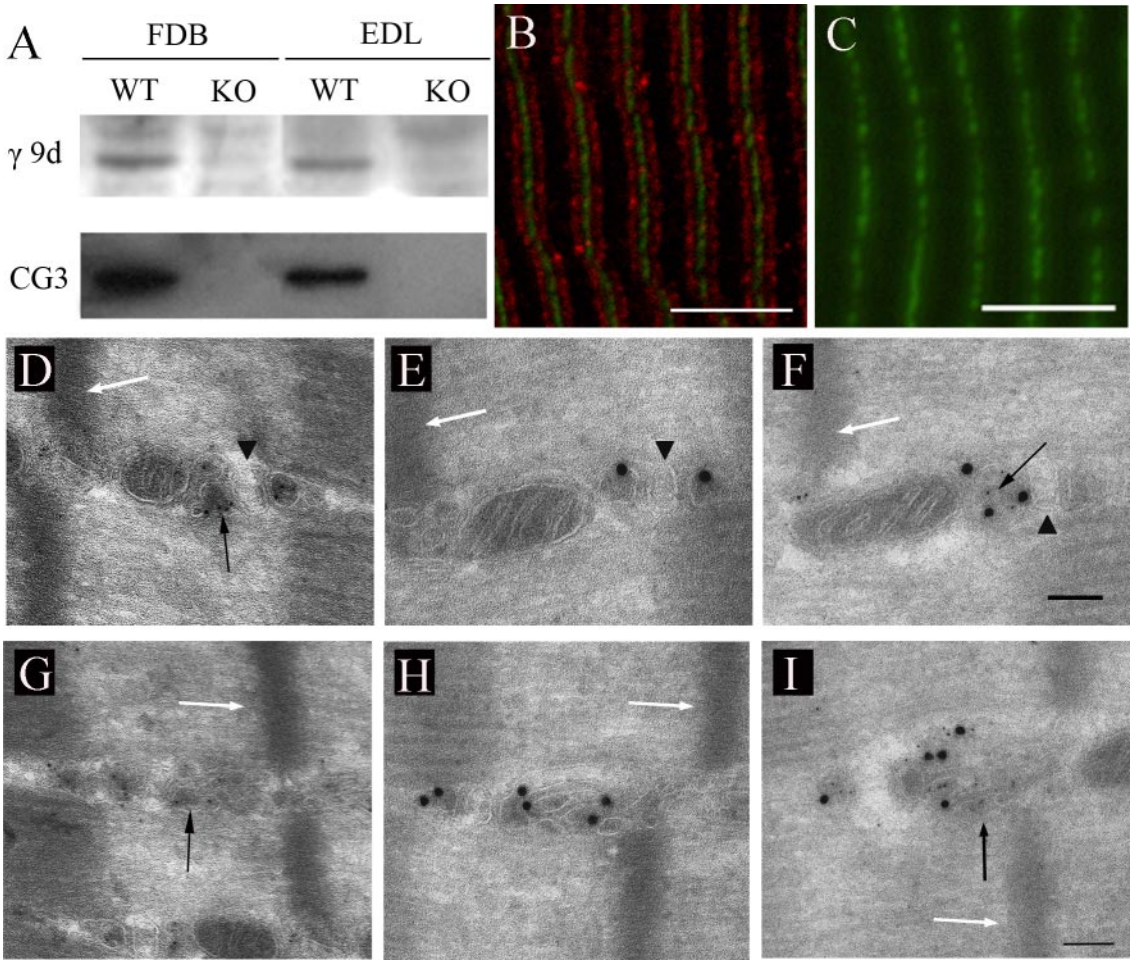

Figure 3. Tm4 does not compensate in the absence of Tm5NM1. Analysis of homozygous Tm5NM1 KO mice (Tm5/9d/89 line) was carried out using Western blotting (A), fluorescent antibody staining (B and C) and immunogold labeling (D–I). (A) Using antibodies to Tm5NM1 (γ9d) Western blotting showed that Tm5NM1 is absent in the FDB and EDL muscles from KO mice. The absence of total cytoskeletal γ-*TM* gene products (recognized by the CG3 antibody) in the KO muscle indicates that other cytoskeletal γ-*TM* isoforms were not up-regulated to compensate for the absence of Tm5NM1. (B and C) Tm5NM1 (red in B) normally located adjacent to the Z-line (α-actinin staining in green in B and C) was absent in semithin sections of EDL muscle from KO mice (C). (D–I) Immunogold labeling of Tm4 (5-nm gold, D and G, arrows) and calsequestrin (20-nm gold, E and H) in EDL muscle from Tm5NM1 KO mice (Tm5/9dneo KO line) was performed. Colabeling (F and I) shows that Tm4 (arrows) remains localized to the terminal SR and tubulovesicular structures in the I-band in the absence of Tm5NM1 and does not localize to the T-tubules. Arrowheads (D–F) point to T-tubule membranes, and Z-lines are labeled with white arrows in D–I. Bars (B and C), 5 μm. Images (D–I) are at the same magnification. Bar (F and I), 100 nm.

Tm5NM1 KO Myofibers Have Altered T-Tubule Function

To define more precisely the mechanism for the altered contractile properties in muscle of the KO mice we performed experiments on single mechanically skinned fibers of KO and WT mice. Maximum Ca^{2+}-activated force was not different in fibers from WT and KO mice ($p > 0.05$; Table 2) in agreement with the isolated intact muscle measurements where maximal tetanic force was unaltered in KO mice. Cooperative binding of Ca^{2+} to the contractile apparatus (n_H) and fiber sensitivity to Ca^{2+}, indicated by Ca^{2+} concentration required for 50% of maximum force (pCa_{50}), were not different between the KO and WT mice (Table 2). Time-to-peak force of Na^+-depolarization force response was decreased in KO fibers (Figure 7A), but relaxation rate was unchanged (data not shown). Importantly, there was no difference in the peak amplitude of the Na^+ depolarization induced force response between KO and WT fibers. These findings are consistent with the data from the isolated intact muscle experiments where time-to-peak twitch force was decreased in the KO mice but the relaxation rate of the twitch response was unchanged (Figure 5, C and D). There was no difference in the ability of the SR to accumulate Ca^{2+} in EDL muscle fibers from WT mice compared with KO mice as evident from the rate constant for SR Ca^{2+} accumulation which was not different between groups ($p > 0.05$; Table 2). Passive SR Ca^{2+} leak and endogenous SR Ca^{2+} levels were also not different in EDL muscle fibers from WT and KO mice (Table 2). Together, the data show that SR function is largely unaltered in the absence of Tm5NM1.

To assess whether loss of Tm5NM1 alters T-tubule function we measured DICR in mechanically skinned fibers from homozygous KO (Tm5/9dneo line) and WT (129X1/SvJ) mice. Fibers were repeatedly depolarized and peak force recorded (Figure 7B). As is evident in Figure 7B, fibers from the KO mice had significantly slower force rundown compared with fibers from WT mice. The time taken to reach 50% of initial force was 7.5 min for the KO and 5.5 min for the WT fibers ($p < 0.05$). The increase in the DICR "rundown" is not due to changes in SR or

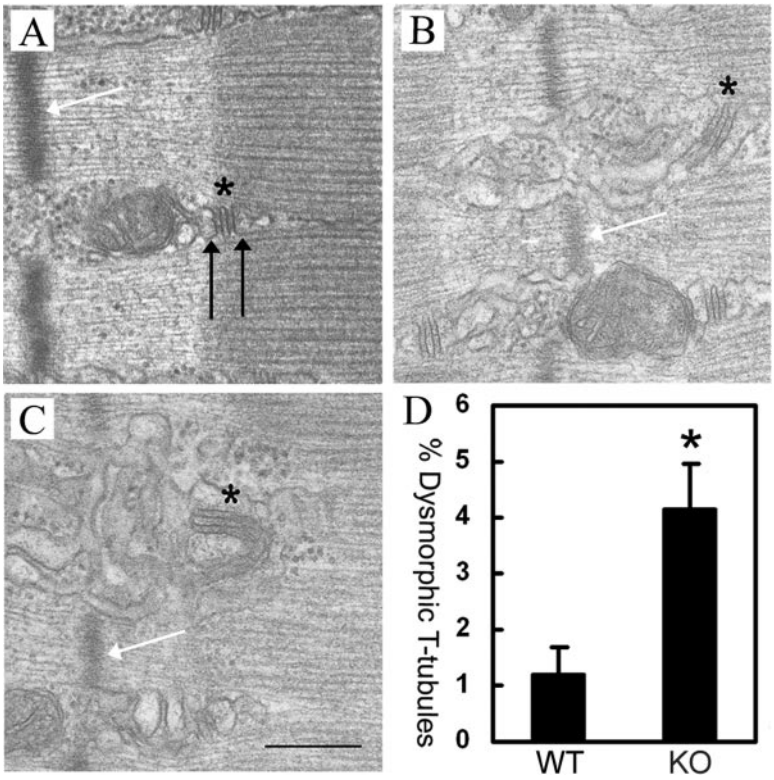

Figure 4. Tm5NM1 KO mice have T-tubule dysmorphology. Analysis of the triads (asterisk in A–C) from WT (A) and homozygous Tm5/9dneo KO (B and C) mouse muscle was carried out using electron microscopy and the number of morphologically abnormal triads quantified (D). The normal triad in WT muscles consists of the T-tubule structure flanked by the terminal SR (A, black arrows). In KO mice, diagonal (B) and bent (C) T-tubule structures were seen more frequently than in WT mice. White arrows in A–C indicate Z-lines. Quantitation (D) showed that the incidence of T-tubule dysmorphology was increased ~3.2-fold in the EDL muscles of KO mice. T-tubule dysmorphology was calculated from a total of 1000 junctional membrane structures from muscles of at least three different mice of each genotype. Data are presented as means ± SE of the mean; *$p < 0.01$ (analysis of variance [ANOVA]). Images A–C are at the same magnification. Bar (C), 500 nm.

contractile properties (Table 2). Therefore, events preceding the opening of the Ca^{2+} channels must be responsible for the increase in T-tubule depolarization-induced responses and likely explain the increase in twitch force and shift in frequency–force curve relationship for isolated intact muscles (Figure 5). These data indicate that loss of Tm5NM1 impacts on muscle contractile performance and that this effect is largely due to dysregulation of T-tubule function.

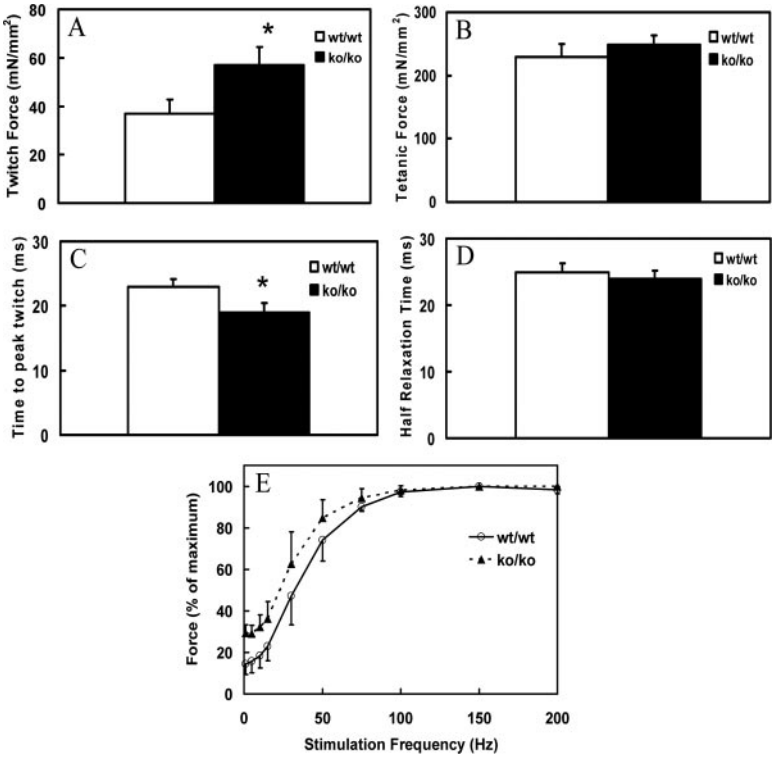

Figure 5. Muscle contractile properties are altered in the Tm5NM1 null mice. Contractile properties of isolated EDL muscles from the Tm5/9dneo KO and WT control (129X1/SvJ strain) mice showing twitch force (A), maximal tetanic force (B; 150 Hz), time to peak twitch force (C), half-relaxation time after twitch contraction (D), and the stimulation–frequency/force relationship (E). There was a significant increase in twitch force (A) (*$p = 0.004$; ANOVA) and decrease in time to peak twitch (C) (*$p = 0.02$) in the EDL muscle from Tm5NM1 KO compared with WT controls. There was a significant "leftward" shift in the frequency force curve (E) such that the forces at 1, 5, 10, and 20Hz ($p < 0.04$) were significantly greater in Tm5NM1 KO mice versus WT controls. Values for all graphs are mean ± SEM ($n = 6–7$) for 10- to 12-wk-old male mice.

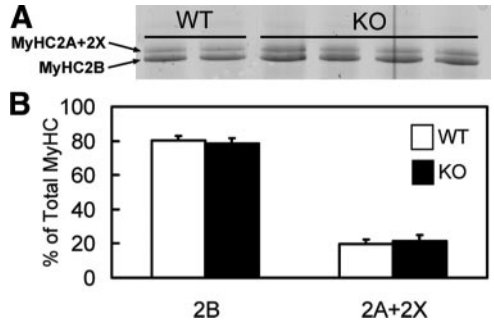

Figure 6. Altered contractile properties in Tm5NM1 null mice are not due to fiber type changes. (A) Representative SDS-PAGE silver-stained gel showing MyHC expression in homozygous WT (129X1/SvJ strain) and KO (Tm5/9dneo) EDL muscles. The MyHC 2A and 2X isoforms migrated as a single band. (B) Quantification of the relative abundance of MyHC isoforms shown in A is based on five to six muscles/genotype. Shown is the MyHC content for each isoform expressed as a percentage of the total MyHC content. Values are mean ± SEM. There was no statistically significant difference in percentage of MyHC content between the WT and KO muscle.

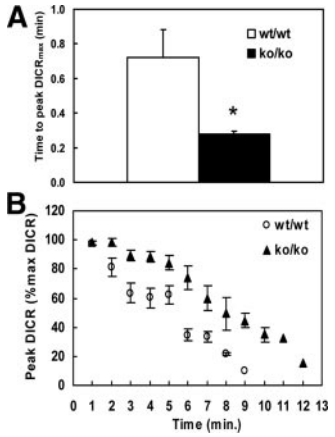

Figure 7. T-tubule function is altered in Tm5NM1 null mice. (A) Time to peak depolarization-induced force was significantly less (*$p < 0.05$) in EDL fibers from homozygous Tm5NM1 KO (Tm5/9dneo line) than WT control (129X1/SvJ) mice. (B) Time course of repeated DICR of mechanically skinned single muscle fiber segments from EDL muscles of homozygous Tm5NM1 KO and WT control mice. The rundown of the DICR in the Tm5NM1 KO mice was significantly slower (time to reach 50% of maximum is significantly different; $p < 0.05$) than the WT mice indicating an increase excitability of the T-tubule system. Values for all graphs are mean ± SEM for 10- to12-wk-old male mice (10–15 fibers from at total of 3 mice of each genotype).

DISCUSSION

Tm5NM1 and Tm4 Define Distinct Structures Adjacent to the Z-Line in Muscle Fibers

In this study, we describe the presence of Tm5NM1- and Tm4-containing filaments in the Z-line adjacent region in skeletal muscle. Tm4 was shown to be localized to the terminal SR, longitudinal SR, and other muscle structures. Tm5NM1 and Tm4 have the ability to form heterodimers in vitro (Temm-Grove *et al*., 1996). However, due to the differences in the Tm5NM1 and Tm4 staining in the immunofluorescent images (Figure 1), it is most likely that these filaments are composed of homodimers of each Tm isoform.

The association of Tm4 with elements of the SR suggests that Tm4-defined actin filaments may have a role in the function of the SR system. Components of the spectrin-ankyrin-actin cytoskeleton have been localized to the SR in cardiac cells (Bennett and Baines, 2001). In erythrocytes, a nonmuscle tropomyosin is a critical element of the spectrin–actin cytoskeleton as without it the integrity of the erythrocyte plasma membrane is severely compromised (An *et al*., 2007). In a similar manner, Tm4 may stabilize an actin–spectrin cytoskeleton in the SR and help maintain the integrity of the SR membrane.

Table 2. Properties of mechanically-skinned single fibers from EDL muscles of WT and Tm5NM1 KO mice

	WT	KO
Maximum Ca^{2+} activated force (kN/m^2)	164.3 ± 6.6 (11)	153.2 ± 5.7 (16)
Ca^{2+} sensitivity (pCa_{50})	5.74 ± 0.01 (9)	5.71 ± 0.01 (11)
Cooperativity (n_H)	5.26 ± 0.33 (10)	5.37 ± 0.33 (14)
SR Ca^{2+} accumulation (m/s)	12.0 ± 7.6 (11)	13.5 ± 6.1 (14)
SR leak (SR Ca^{2+} lost in 60 s)	25.9 ± 4.6 (9)	29.1 ± 5.9 (10)
Endogenous SR Ca^{2+} (mM)	1.38 ± 0.49 (11)	1.73 ± 0.59 (16)

Results are for EDL fibers from the Tm5/9dneo KO line and WT control strain (129X1/SvJ). Values are mean ± SEM and the number fibers measured are in parentheses. There was no significant difference ($p > 0.05$) between KO and WT control fibers for any parameter.

Tm5NM1 Impacts on the Structure of the T-Tubules

The accurate formation and alignment of the T-tubules and SR systems as well as preservation of the structure of these elements is critical to muscle function. The development and maturation of the SR and T-tubules takes place over several weeks and occurs in three discrete steps: 1) the independent differentiation of the membrane compartments of the T-tubules and SR, 2) the formation of the SR/T-tubule junctional triad, and 3) the alignment of the triads with the myofibrils and the transverse orientation of the T-tubules (Flucher *et al*., 1992; Takekura *et al*., 2001). Many molecules have been implicated in the formation of the triad junction and the physical coupling of the SR with the T-tubule membrane (e.g., amphiphysin 2, junctophilins, and mitsugumin 29) (Takeshima *et al*., 2000; Ito *et al*., 2001; Komazaki *et al*., 2001, 2002; Razzaq *et al*., 2001; Lee *et al*., 2002). The junctophilins in particular have been shown to be critical for the proper alignment of the T-tubule/SR membranes (Takeshima *et al*., 2000; Komazaki *et al*., 2002). This is thought to be mediated through interactions with proteins associated with the junctional SR (ryanodine receptor and triadin), suggesting that there is a protein network that organizes the localization of junctional proteins. Three independent cytoskeletal systems also exist at the T-tubule/SR membranes: the vinculin/talin/integrin complex, the dystrophin-glycoprotein complex and the spectrin-based membrane skeleton (Hoffman *et al*., 1987; Knudson *et al*., 1988; Kostin *et al*., 1998) and their absence leads to altered T-tubule morphology (Oguchi *et al*., 1982). In this study, the absence of Tm5NM1 led to a small increase in abnormally shaped T-tubules. This raises the possibility that the actin filament system has a role in maintenance of T-tubule membrane structure. The importance of cytoskeletal Tms in maintaining the structure and function of membrane structures has been recently shown in

osteoclasts where knockdown of Tm4 resulted in changes in podosome shape and diminished bone resorptive capacity (McMichael and Lee, 2008).

Tm5NM1 Regulates T-Tubule Function

The T-tubule system is responsible for the propagation of the action potential from the sarcolemma of the muscle fiber to the contractile units. The T-tubules connect with the sarcoplasmic reticulum to form the triad and initiate the release of calcium for sarcomeric contraction. Altered excitation-contraction (E-C) coupling is a consistent feature of mice null for proteins located at the triad junction. This includes not only proteins involved directly in the process of E-C coupling (ryanodine receptor and dihydropyridine receptor) but also proteins involved in the formation of the triad junctional membrane complex (Takeshima *et al*., 1998, 2000; Razzaq *et al*., 2001). Tm5NM1 KO mice exhibit an alteration in contractile function consistent with changes to E-C coupling (increased twitch force, increase in the excitability as measured by repeated depolarization-induced force responses). It is unclear whether this is due to changes in the expression of components of the E-C coupling apparatus or some direct regulatory effect of the actin cytoskeleton on the process of E-C coupling.

We have shown that the increase in DICRs in Tm5NM1 KO muscle is not due to changes in SR function or contractile properties (Table 1) and the small increase in dysmorphic T-tubules in the KO (4%) does not account for this dysfunction. As endogenous Ca^{2+} in the SR (Table 1) and SR morphology were unaltered in the KO muscle it is unlikely that an increase in SR volume is responsible for the contractile phenotype. It would seem therefore that events preceding Ca^{2+} release from the SR are responsible for the altered T-system responses and presumably the increased twitch force. This could include 1) quicker repolarization of the T-tubule membranes in KO fibers, perhaps due to altered Na^{+}/K^{+} pump function; 2) increased sensitivity of the DHPR (L-type Ca^{2+} channel) to change in voltage; or 3) greater ability of KO fibers to transfer the electrical signal to the ryanodine receptor triggering greater Ca^{2+} release.

We have shown that Tm5NM1 and Tm4 define independent γ-actin filament populations within the myofiber (Kee *et al*., 2004; Vlahovich *et al*., 2008). γ-Actin has also been shown to be part of the juxtamembrane complex, the costamere (Craig and Pardo, 1983; Rybakova *et al*., 2000), that is thought to provide a link between the dystroglycan complex and the sarcomeric Z-line (Rybakova *et al*., 2000). Surprisingly, ablation of this actin isoform in KO mouse muscle did not result in dystrophy, but a progressive breakdown of muscle (necrosis and regeneration) with features similar to centronuclear myopathy (Sonnemann *et al*., 2006). These mice are weak, have decreased twitch force and decreased action-potential evoked Ca^{2+} release. The authors attributed these contractile defects to increased mechanical compliance caused by altered connectivity between muscle fibers and/or myofibrils at the myotendinous junction. However, the data from the Tm5NM1 KO mouse in the present study suggests that the contractile defects in γ-actin KO muscle could be due to at least in part alterations to T-tubule/SR function.

CONCLUSIONS

Tms are known to form functionally distinct compartments in a range of cell types (Gunning *et al*., 2008). This study shows that skeletal muscle contains two cytoskeletal Tm isoforms, Tm5NM1 and Tm4, that compartmentalize to define independent actin filaments in association with internal membrane systems in skeletal muscle. Loss of Tm5NM1 in skeletal muscle resulted in contractile defects consistent with altered T-tubule function. In osteoclasts, knockdown of Tm4 results in changes in podosome shape and diminished bone resorptive capacity indicating the importance of this Tm in maintaining the structure and function of membrane structures (McMichael and Lee, 2008). Together, these studies suggest specific, independent roles for the Tm isoforms in association with different membrane structures.

ACKNOWLEDGMENTS

We thank the staff of the Electron Microscope Laboratory (a joint facility of the Institute of Clinical Pathology and Medical Research and the Westmead Research Hub), especially Ross Boadle for expert advice with immunolabeling techniques. This work was supported by Australian National and Medical Research Council (NHMRC) grants 321705 (to P.W.G., E.C.H., and A.J.K.) and 511005 (to R.G.P.) and by funding from the Oncology Children's Foundation (to P.W.G.). P.W.G. and R.G.P. are Principal Research Fellows of the NHMRC (grant 163626 and 351411, respectively).

REFERENCES

An, X., Salomao, M., Guo, X., Gratzer, W., and Mohandas, N. (2007). Tropomyosin modulates erythrocyte membrane stability. Blood *109*, 1284–1288.

Bennett, V., and Baines, A. J. (2001). Spectrin and ankyrin-based pathways: metazoan inventions for integrating cells into tissues. Physiol. Res. *81*, 1353–1492.

Bernstein, B. W., and Bamburg, J. R. (1982). Tropomyosin binding to F-actin protects the F-actin from disassembly by brain actin-depolymerizing factor (ADF). Cell Motil. *2*, 1–8.

Bryce, N. S. *et al*. (2003). Specification of actin filament function and molecular composition by tropomyosin isoforms. Mol. Biol. Cell *14*, 1002–1016.

Craig, S. W., and Pardo, J. V. (1983). Gamma actin, spectrin, and intermediate filament proteins colocalize with vinculin at costameres, myofibril-to-sarcolemma attachment sites. Cell Motil. *3*, 449–462.

Dalby-Payne, J. R., O'Loughlin, E. V., and Gunning, P. (2003). Polarization of specific tropomyosin isoforms in gastrointestinal epithelial cells and their impact on CFTR at the apical surface. Mol. Biol. Cell *14*, 4365–4375.

Fanning, A. S., Wolenski, J. S., Mooseker, M. S., and Izant, J. G. (1994). Differential regulation of skeletal muscle myosin-II and brush border myosin-I enzymology and mechanochemistry by bacterially produced tropomyosin isoforms. Cell Motil. Cytoskeleton *29*, 29–45.

Flucher, B. E., Phillips, J. L., Powell, J. A., Andrews, S. B., and Daniels, M. P. (1992). Coordinated development of myofibrils, sarcoplasmic reticulum and transverse tubules in normal and dysgenic mouse skeletal muscle, in vivo and in vitro. Dev. Biol. *150*, 266–280.

Gregorevic, P., Plant, D. R., and Lynch, G. S. (2004). Administration of insulin-like growth factor-I improves fatigue resistance of skeletal muscles from dystrophic mdx mice. Muscle Nerve *30*, 295–304.

Griffiths, G., McDowall, A., Back, R., and Dubochet, J. (1984). On the preparation of cryosections for immunocytochemistry. J. Ultrastruct. Res. *89*, 65–78.

Gunning, P. W., O'Neill, G., and Hardeman, E. C. (2008). Tropomyosin-based regulation of the actin cytoskeleton in time and space. Physiol. Rev. *88*, 1–35.

Had, L., Faivre-Sarrailh, C., Legrand, C., and Rabie, A. (1993). The expression of tropomyosin genes in pure cultures of rat neurons, astrocytes and oligodendrocytes is highly cell-type specific and strongly regulated during development. Brain Res. Mol. Brain Res. *18*, 77–86.

Hannan, A. J., Gunning, P., Jeffrey, P. L., and Weinberger, R. P. (1998). Structural compartments within neurons: developmentally regulated organization of microfilament isoform mRNA and protein. Mol. Cell. Neurosci. *11*, 289–304.

Hannan, A. J., Schevzov, G., Gunning, P., Jeffrey, P. L., and Weinberger, R. P. (1995). Intracellular localization of tropomyosin mRNA and protein is associated with development of neuronal polarity. Mol. Cell. Neurosci. *6*, 397–412.

Hernandez-Deviez, D. J., Martin, S., Laval, S. H., Lo, H. P., Cooper, S. T., North, K. N., Bushby, K., and Parton, R. G. (2006). Aberrant dysferlin trafficking in cells lacking caveolin or expressing dystrophy mutants of caveolin-3. Hum. Mol. Genet. *15*, 129–142.

Hoffman, E. P., Knudson, C. M., Campbell, K. P., and Kunkel, L. M. (1987). Subcellular fractionation of dystrophin to the triads of skeletal muscle. Nature *330*, 754–758.

Ishikawa, R., Yamashiro, S., and Matsumura, F. (1989). Annealing of gelsolin-severed actin filaments by tropomyosin in the presence of Ca^{2+}. Potentiation of the annealing process by caldesmon. J. Biol. Chem. *264*, 16764–16770.

Ito, K., Komazaki, S., Sasamoto, K., Yoshida, M., Nishi, M., Kitamura, K., and Takeshima, H. (2001). Deficiency of triad junction and contraction in mutant skeletal muscle lacking junctophilin type 1. J. Cell Biol. *154*, 1059–1067.

Joya, J. E., Kee, A. J., Nair-Shalliker, V., Ghoddusi, M., Nguyen, M. A., Luther, P., and Hardeman, E. C. (2004). Muscle weakness in a mouse model of nemaline myopathy can be reversed with exercise and reveals a novel myofiber repair mechanism. Hum. Mol. Genet. *13*, 2633–2645.

Kee, A. J. *et al*. (2004). Sorting of a nonmuscle tropomyosin to a novel cytoskeletal compartment in skeletal muscle results in muscular dystrophy. J. Cell Biol. *166*, 685–696.

Komazaki, S., Ito, K., Takeshima, H., and Nakamura, H. (2002). Deficiency of triad formation in developing skeletal muscle cells lacking junctophilin type 1. FEBS Lett. *524*, 225–229.

Komazaki, S., Nishi, M., and Takeshima, H. (2003). Abnormal junctional membrane structures in cardiac myocytes expressing ectopic junctophilin type 1. FEBS Lett. *542*, 69–73.

Komazaki, S., Nishi, M., Takeshima, H., and Nakamura, H. (2001). Abnormal formation of sarcoplasmic reticulum networks and triads during early development of skeletal muscle cells in mitsugumin 29-deficient mice. Dev. Growth Differ. *43*, 717–723.

Kostin, S., Scholz, D., Shimada, T., Maeno, Y., Mollnau, H., Hein, S., and Schaper, J. (1998). The internal and external protein scaffold of the T-tubular system in cardiomyocytes. Cell Tissue Res. *294*, 449–460.

Knudson, C. M., Hoffman, E. P., Kahl, S. D., Kunkel, L. M., and Campbell, K. P. (1988). Evidence for the association of dystrophin with the transverse tubular system in skeletal muscle. J. Biol. Chem. *263*, 8480–8484.

Lee, E., Marcucci, M., Daniell, L., Pypaert, M., Weisz, O. A., Ochoa, G. C., Farsad, K., Wenk, M. R., and De Camilli, P. (2002). Amphiphysin 2 (Bin1) and T-tubule biogenesis in muscle. Science *297*, 1193–1196.

Lynch, G. S., Hinkle, R. T., Chamberlain, J. S., Brooks, S. V., and Faulkner, J. A. (2001). Force and power output of fast and slow skeletal muscles from mdx mice 6–28 months old. J. Physiol. *535*, 591–600.

McMichael, B. K., and Lee, B. S. (2008). Tropomyosin 4 regulates adhesion structures and resorptive capacity in osteoclasts. Exp. Cell Res. *314*, 564–573.

Oguchi, K., Yanagisawa, N., and Tsukagoshi, H. (1982). The structure of the T-system in human muscular dystrophy. A high-voltage electron-microscopic study. J. Neurol. Sci. *57*, 333–341.

Ono, S., and Ono, K. (2002). Tropomyosin inhibits ADF/cofilin-dependent actin filament dynamics. J. Cell Biol. *156*, 1065–1076.

Nair-Shalliker, V., Kee, A. J., Joya, J. E., Lucas, C. A., Hoh, J. F., and Hardeman, E. C. (2004). Myofiber adaptational response to exercise in a mouse model of nemaline myopathy. Muscle Nerve *30*, 470–480.

Percival, J. M., Hughes, J. A., Brown, D. L., Schevzov, G., Heimann, K., Vrhovski, B., Bryce, N., Stow, J. L., and Gunning, P. W. (2004). Targeting of a tropomyosin isoform to short microfilaments associated with the Golgi complex. Mol. Biol. Cell *15*, 268–280.

Perry, S. V. (2001). Vertebrate tropomyosin: distribution, properties and function. J. Muscle Res. Cell Motil. *22*, 5–49.

Plant, D. R., and Lynch, G. S. (2002). Excitation-contraction coupling and sarcoplasmic reticulum function in mechanically skinned fibres from fast skeletal muscles of aged mice. J. Physiol. *543*, 169–176.

Razzaq, A., Robinson, I. M., McMahon, H. T., Skepper, J. N., Su, Y., Zelhof, A. C., Jackson, A. P., Gay, N. J., and O'Kane, C. J. (2001). Amphiphysin is necessary for organization of the excitation-contraction coupling machinery of muscles, but not for synaptic vesicle endocytosis in Drosophila. Genes Dev. *15*, 2967–2979.

Rybakova, I. N., Patel, J. R., and Ervasti, J. M. (2000). The dystrophin complex forms a mechanically strong link between the sarcolemma and costameric actin. J. Cell Biol. *150*, 1209–1214.

Saito, A., Seiler, S., Chu, A., and Fleischer, S. (1984). Preparation and morphology of sarcoplasmic reticulum terminal cisternae from rabbit skeletal muscle. J. Cell Biol. *99*, 875–885.

Schevzov, G. *et al*. (2008). Divergent regulation of the sarcomere and the cytoskeleton. J. Biol. Chem. *283*, 275–283.

Schevzov, G., Bryce, N. S., Almonte-Baldonado, R., Joya, J., Lin, J. J., Hardeman, E., Weinberger, R., Gunning, P. (2005a). Specific features of neuronal size and shape are regulated by tropomyosin isoforms. Mol. Biol. Cell *16*, 3425–3437.

Schevzov, G., Gunning, P., Jeffrey, P. L., Temm-Grove, C., Helfman, D. M., Lin, J. J., and Weinberger, R. P. (1997). Tropomyosin localization reveals distinct populations of microfilaments in neurites and growth cones. Mol. Cell. Neurosci. *8*, 439–454.

Schevzov, G., Vrhovski, B., Bryce, N. S., Elmir, S., Qiu, M. R., O'Neill, G. M., Yang, N., Verrills, N. M., Kavallaris, M., and Gunning, P. W. (2005b). Tissue-specific tropomyosin isoform composition. J. Histochem. Cytochem. *53*, 557–570.

Schwenk, F., Baron, U., and Rajewsky, K. (1995). A cre-transgenic mouse strain for the ubiquitous deletion of loxP-flanked gene segments including deletion in germ cells. Nucleic Acids Res. *25*, 5080–5081.

Smith, J. P., Hicks, P. S., Ortiz, L. R., Martinez, M. J., and Mandler, R. N. (1995). Quantitative measurement of muscle strength in the mouse. J. Neurosci. Methods *62*, 15–19.

Sonnemann, K. J., Fitzsimons, D. P., Patel, J. R., Liu, Y., Schneider, M. F., Moss, R. L., and Ervasti, J. M. (2006). Cytoplasmic gamma-actin is not required for skeletal muscle development but its absence leads to a progressive myopathy. Dev. Cell *11*, 387–397.

Stephenson, D. G., and Williams, D. A. (1981). Calcium-activated force responses in fast- and slow-twitch skinned muscle fibres of the rat at different temperatures. J. Physiol. *317*, 281–302.

Takekura, H., Flucher, B. E., and Franzini-Armstrong, C. (2001). Sequential docking, molecular differentiation, and positioning of T-Tubule/SR junctions in developing mouse skeletal muscle. Dev. Biol. *239*, 204–214.

Takeshima, H., Komazaki, S., Nishi, M., Iino, M., and Kangawa, K. (2000). Junctophilins: a novel family of junctional membrane complex proteins. Mol. Cell *6*, 11–22.

Takeshima, H., Shimuta, M., Komazaki, S., Ohmi, K., Nishi, M., Iino, M., Miyata, A., and Kangawa, K. (1998). Mitsugumin29, a novel synaptophysin family member from the triad junction in skeletal muscle. Biochem. J. *331*, 317–322.

Tang, N., and Ostap, E. M. (2001). Motor domain-dependent localization of myo1b (myr-1). Curr. Biol. *11*, 1131–1135.

Temm-Grove, C. J., Guo, W., and Helfman, D. M. (1996). Low molecular weight rat fibroblast tropomyosin 5 (TM-5): cDNA cloning, actin-binding, localization, and coiled-coil interactions. Cell Motil. Cytoskeleton *33*, 223–240.

van der Poel, C., and Stephenson, D. G. (2002). Reversible changes in Ca(2+)-activation properties of rat skeletal muscle exposed to elevated physiological temperatures. J. Physiol. *544*, 765–776.

van der Poel, C., and Stephenson, D. G. (2007). Effects of elevated physiological temperatures on sarcoplasmic reticulum function in mechanically skinned muscle fibers of the rat. Am. J. Physiol. Cell Physiol. *293*, C133–C141.

Vlahovich, N., Schevzov, G., Nair-Shaliker, V., Ilkovski, B., Artap, S. T., Joya, J. E., Kee, A. J., North, K. N., Gunning, P. W., and Hardeman, E. C. (2008). Tropomyosin 4 defines novel filaments in skeletal muscle associated with muscle remodelling/regeneration in normal and diseased muscle. Cell Motil. Cytoskeleton *65*, 73–85.

Weinberger, R. P., Henke, R. C., Tolhurst, O., Jeffrey, P. L., and Gunning, P. (1993). Induction of neuron-specific tropomyosin mRNAs by nerve growth factor is dependent on morphological differentiation. J. Cell Biol. *120*, 205–215.